

Probing $\text{La}_{0.7}\text{Sr}_{0.3}\text{MnO}_3$ multilayers via spin wave resonances

Rhet Magaraggia,* Mikhail Kostylev, and Robert L Stamps
*School of Physics, University of Western Australia,
 35 Stirling Highway, Crawley, Western Australia 6009, Australia*

Michael Hambe and Valanoor Nagarajan
School of Materials Science and Engineering University of New South Wales NSW 2052, Australia

$\text{La}_{0.7}\text{Sr}_{0.3}\text{MnO}_3/\text{BiFeO}_3$ and $\text{La}_{0.7}\text{Sr}_{0.3}\text{MnO}_3/\text{PbZr}_{20}\text{Ti}_{80}\text{O}_3$ epitaxial heterostructures have been grown on SrTiO_3 substrates. Spin wave resonances are used to study interface properties of the ferromagnetic $\text{La}_{0.7}\text{Sr}_{0.3}\text{MnO}_3$. We find that the addition of the BiFeO_3 or $\text{PbZr}_{20}\text{Ti}_{80}\text{O}_3$ causes out-of-plane surface pinning of the $\text{La}_{0.7}\text{Sr}_{0.3}\text{MnO}_3$. We are able to place new limits on the exchange constant D of $\text{La}_{0.7}\text{Sr}_{0.3}\text{MnO}_3$ grown on these substrates and confirm the presence of uniaxial and biaxial anisotropies caused by the SrTiO_3 substrate.

I. INTRODUCTION

The promise of electrically and magnetically tunable tunnel junctions for use in both spin valves and four state memory devices[1–3], is an exciting prospect. $\text{La}_{1-x}\text{Sr}_x\text{MnO}_3/\text{BiFeO}_3$ (LSMO/BFO) multilayers are proposed for spin valve devices, as LSMO has demonstrated good spin filtering properties[4] and BFO is a room temperature multiferroic which could, in principle, provide an electrically tunable exchange biased film[5–7]. Both of these materials are perovskite based structures and have small lattice mismatch when grown on a suitable substrate. Practically, it is important to understand how the magnetization of LSMO films is affected when epitaxially joined to a ferroelectric. Enhancement of uniaxial anisotropies, development of unidirectional anisotropies, surface pinning from the interface and changes to other micromagnetic parameters are all important characteristics with respect to tunnel junction performance. Though most of these properties have been explored in single layer LSMO[8–16], the effects of ferroelectric overlayers can be important and have begun to be studied[17, 18]. In this paper we examine pinning of dynamic magnetization using spin wave measurements. A new result is our measure for the spin wave exchange constant D . To the best of the authors knowledge, only four other measurements of D have been carried out so far[11, 19–21], and only one study which utilises standing spin wave modes for determination of D [11]. We also use standing spin wave resonances to measure anisotropies caused by both the ferroelectric overlayer and growth of LSMO on a single crystal substrate.

II. STANDING SPIN WAVE MODES

A powerful technique to probe magnetic conditions at buried interfaces is through spin wave resonances[22–26].

The structure of standing spin wave modes contains detailed information about bulk magnetic properties, such as gyromagnetic ratio γ and exchange constant D , and also provides information about interfacial pinning of the magnetization vector.

The ferromagnetic resonance frequency for out-of-plane magnetized thin films is

$$\frac{\omega}{\gamma} = H_{eff} + H_R \quad (1)$$

where $H_{eff} = -\mu_0 M_S + H_{oop} + D k_{oop}^2$, ω is the precession frequency, γ is the gyromagnetic ratio, H_R is the externally applied field, $\mu_0 M_S$ is the demagnetizing field due to the out-of-plane alignment of spins, H_{oop} is any bulk out-of-plane anisotropy field and $D k_{oop}^2$ is the exchange energy of the standing spin wave mode. Measurement of multiple modes allows determination of γ and H_{eff} . Separation of $-\mu_0 M_S + H_A$ and $D k_{oop}^2$, is possible when the fundamental resonance mode frequency (FMR mode) and the first exchange mode (FEX mode) are measured. Due to the shorter wavelength and much higher energy density of the FEX mode, any changes in wavelength due to surface pinning strongly affect the frequency gap between the FEX and FMR modes.

Subtraction of the effective field data of the FEX mode $H_{eff}(FEX)$, from the FMR mode $H_{eff}(FMR)$ gives us a measure of the strength of pinning and the exchange constant. By rotating the film in-plane and taking angular measurements, the angular variation of pinning and bulk anisotropies may be determined.

Angular dependence of spin wave frequencies for in plane magnetization can be used to measure magnetocrystalline anisotropies. The Kittel formula describing resonance conditions for the magnetization oriented in-plane is[24]

$$\left(\frac{\omega}{\gamma}\right)^2 = (H_R(\theta) + \mu_0 M_S - H_{oop} + H_{ip}(\theta) + D k_{ip}^2(\theta)) \times (H_R(\theta) + H_{ip}(\theta) + D k_{ip}^2(\theta)) \quad (2)$$

* rhet.magaraggia@gmail.com

Here H_{ip} is the in-plane bulk anisotropy and k_{ip}^2 refers to the wave vector of standing wave modes with magnetization aligned in plane. We make distinct k_{ip}^2 and k_{oop}^2 which need not in general be the same depending upon pinning conditions at the film interface. Also included is an angular dependence θ which denotes the magnetization direction with respect to some arbitrary in-plane film direction.

The paper is structured as follows. We first describe sample growth and characterization, and the ferromagnetic resonance experiment. FMR results are presented along with a discussion of bulk and surface anisotropies. We conclude with results for the exchange constant D of $\text{La}_{1-x}\text{Sr}_x\text{MnO}_3$ films.

III. SAMPLE GROWTH AND CHARACTERIZATION

A series of films comprising epitaxial $\text{La}_{0.7}\text{Sr}_{0.3}\text{MnO}_3$ (LSMO) were grown on single crystal (100) orientated SrTiO_3 (STO) substrates, with the addition of either an epitaxial BiFeO_3 (BFO) or $\text{PbZr}_{20}\text{Ti}_{80}\text{O}_3$ (PZT) capping layer. As a comparison, a thick polycrystalline LSMO film was grown on MgAl_2O_4 . All films were grown via Pulsed Laser Deposition (PLD) with a KrF excimer laser at 248 nm with laser fluency of $\sim 2 \text{ J cm}^{-2}$. The STO substrates were sourced from Shinkosa Co. LTD Japan with a manufacturers claim of less than 0.3° miscut, and arrived pre-etched to provide a TiO_2 terminated surface. All substrates were sonicated in isopropyl alcohol to remove organic contaminants before use. The deposition chamber base pressure was better than 5.0×10^{-7} Torr before the sample was heated to deposition temperature and a partial oxygen pressure was introduced. LSMO films were deposited at 700 degrees Celsius with an oxygen partial pressure of 100 mT, repetition rate of 10Hz, laser fluence of 1.8 J cm^{-2} and were cooled under 300 Torr O_2 at 5 degrees per minute. BFO films were deposited at 700 degrees Celsius with an oxygen partial pressure of 5 mT, repetition rate of 20Hz, laser fluence of 1.6 J cm^{-2} and were cooled under 220 Torr O_2 at 5 degrees per minute. PZT films were deposited at 550 degrees Celsius with an oxygen partial pressure of 100 mT, repetition rate of 3 Hz, laser fluence of 1.6 J cm^{-2} and were cooled under 700 Torr O_2 at 5 degrees per minute. The growth rate of LSMO, BFO and PZT were $\sim 0.002 \text{ nm/pulse}$, $\sim 0.004 \text{ nm/pulse}$ and $\sim 0.002 \text{ nm/pulse}$ respectively. LSMO and BFO phase purity was confirmed via standard X-Ray diffraction on a Philips Xpert Pro MRD system. An example is shown in Fig. (1).

The LSMO thickness was calibrated via X-Ray reflectivity measurements on a Philips Xpert Pro MRD system. The BFO thickness was calibrated via TEM analysis, as published in[27]. Our samples exhibit low surface roughness, less than 2.6\AA rms, indicating smooth growth as shown in Fig.(1).

A step pattern is seen which exists in the underlying

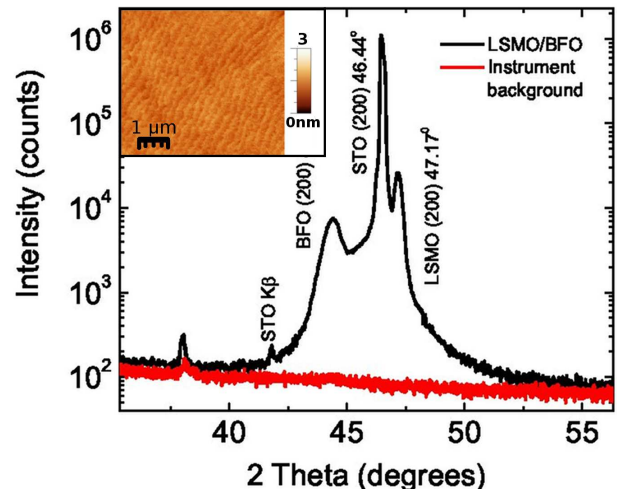


FIG. 1. A characteristic XRD image of the LSMO(55nm)/BFO(18nm) film showing excellent phase purity. The inset demonstrates the step structure imaged with AFM which originates on the surface of the of the LSMO(38.9nm) sample due to epitaxial growth in on top of the stepped substrate.

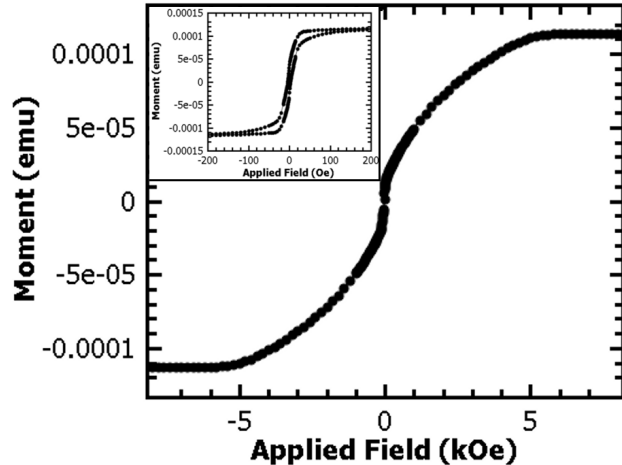


FIG. 2. SQUID data taken at room temperature with the field applied out of the film plane, inset displays the SQUID hysteresis at for the field applied in the plane of the film

STO substrates and is preserved throughout the LSMO epitaxial growth. In-plane and out-of-plane SQUID magnetometry was performed, and from this data (seen in Fig.(2)) $\mu_0 M_S - H_{oop}$ was determined to be $\sim 0.5 \pm 0.05 \text{ T}$.

IV. FERROMAGNETIC RESONANCE

The FMR characterisation was done using a Vector Network Analyser (VNA) and Field-Modulated (FM) FMR setups. The VNA-FMR is used to obtain S21 parameters from field swept measurements as discussed in [28]. It consists of a Danphysik power supply to drive the electromagnets, and an Agilent N5230 PNA-L vector network analyser operating in a 1-20GHz frequency range. The FM-FMR setup uses the VNA as the microwave source, and an SRS SR850 lock-in amplifier and HP 33120A function generator to drive the field modulated measurements. In both cases a 0.3mm microstrip waveguide was used as the microwave antenna source as shown in Fig.(3). The sample is placed with the film in direct contact with the microstrip.

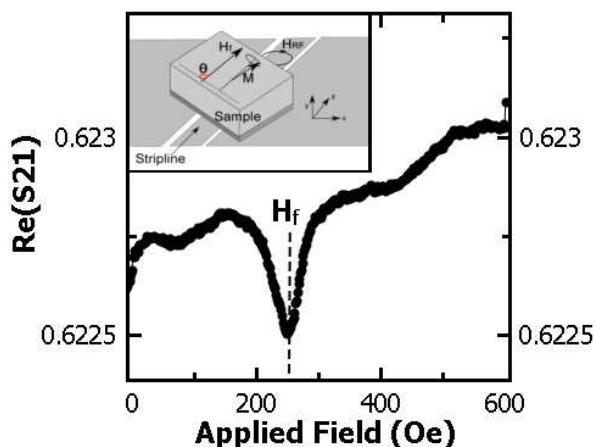


FIG. 3. Raw data from VNA-FMR sweep for the LSMO(38.86nm) film in the 0° with a 3GHz driving microwave field. As the applied field is swept, the $\text{Re}(S_{21})$ parameter is measured (shown on y-axis) and when resonance occurs at H_f there is a marked change in the $\text{Re}(S_{21})$ coefficient. Inset displays a close picture of the in-plane experimental setup with the sample sitting on top of a stripline, M is the magnetisation precessing in response to the driving microwave field H_{RF} and the entire sample has its orientation varied by θ with respect to the external field H_f .

The in-plane FMR procedure for extracting resonance conditions is as follows. The frequency is constant, and an external magnetic field is swept while the S21 transmission coefficients are measured. This procedure is repeated for several different frequencies. An example result is shown in Fig.(3).

V. FMR RESULTS AND DISCUSSION

Only the FMR resonance was observed for the in-plane configuration. Lack of FEX mode absorption may correspond to weak surface pinning in the plane of the film. If surface pinning is weak, then the FEX mode has a symmetric magnetisation profile across the film thickness,

producing no net dipole moment to couple to[25]. In this case, only a non-uniform driving field, caused for example by eddy currents in a conducting sample, can drive resonance[29–33]. Due to the low conductivity of LSMO compared to Permalloy, we do not expect significant non-uniformity of driving field across the sample thicknesses studied. Hence the FEX mode visibility should originate primarily from intrinsic surface pinning.

Magnetocrystalline anisotropies can be determined for angular measurements in-plane, as noted above. The results for an angular study of just the FMR mode is displayed in Fig.(4).

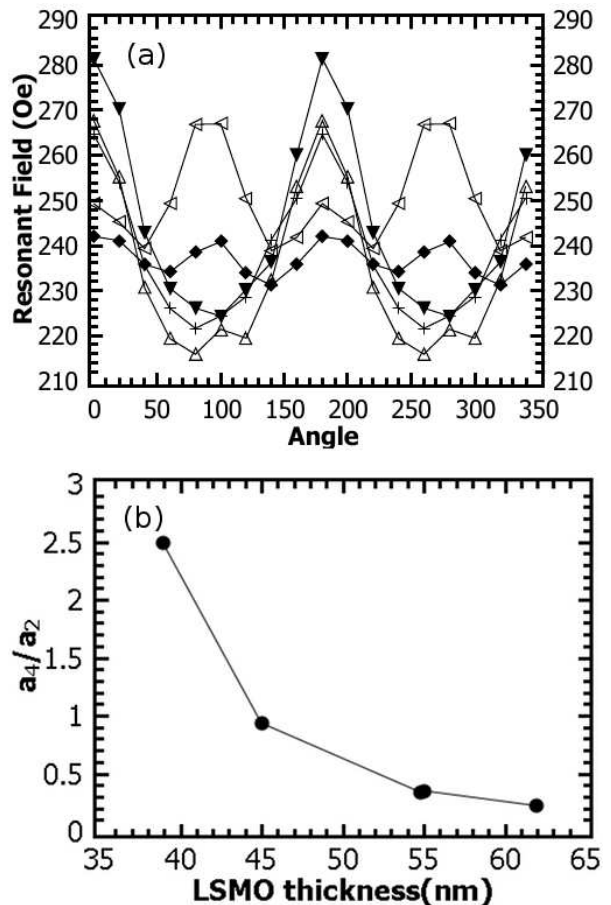


FIG. 4. (a) Displayed is a plot showing the resonant field H_f as a function of film angle θ , all experiments used a 3GHz driving microwave field: LSMO(38.89nm) (solid diamond line), LSMO(45nm)/PZT(20nm) (empty sideways triangle line), LSMO(54.8nm)/BFO(23nm) (solid triangle line), LSMO(61.9nm) (cross line), LSMO(55nm)/BFO(18nm) (empty upright triangles). The thinnest LSMO film clearly displays anisotropy of a biaxial character, whereas the thickest LSMO films have a uniaxial character. Interestingly the 45nm LSMO film displays a mixing of both anisotropy types. (b) shows how the ratio of biaxial (a_4) to uniaxial (a_2) contributions from Eq.(3) vary as a $\frac{1}{t}$ LSMO thickness dependence.

The type of anisotropy seems to be dependent on the film thickness. Biaxial and uniaxial anisotropies can be

identified with the thinnest LSMO film having a biaxial character and the thickest LSMO films having a uniaxial character. There is also the case of the intermediate 45nm LSMO film which displays an unequal mixing of both uniaxial and biaxial character. Quantitative information on the form of the angular anisotropies can be obtained by fitting to:

$$H_R = a_0 + a_2 \sin(2\theta + \phi_1) + a_4 \sin(4\theta + \phi_2) \quad (3)$$

where H_R is the resonant applied field, θ is the film angle with respect to the applied field, a_2 is a uniaxial anisotropy term, a_4 is a biaxial anisotropy term. The ϕ are phase shifts of the anisotropies with respect to the 0° measurement direction. Examining the ratio $\frac{a_2}{a_4}$ as a function of LSMO thickness reveals a $\frac{1}{t}$ trend as shown in Fig.(4). This indicates that the uniaxial anisotropy dominates over the biaxial anisotropy as the LSMO thickness increases. Furthermore, this effect is related to the LSMO and substrate, as it does not appear to be correlated with the capping layer.

Previous studies have noted both uniaxial and biaxial anisotropies present in STO/LSMO films, with the biaxial anisotropy originating from the cubic symmetries of epitaxial LSMO grown on (001) STO and the uniaxial anisotropies originating from physical steps on the STO surface[13, 34–36]. It was reported that the in-plane four-fold and two-fold anisotropies are bulk in origin and not strongly related to interface pinning.

It should be noted however that both anisotropies are established during the growth process. In particular, because we measure a strong uniaxial anisotropy for quite thick (60nm) LSMO films, it would seem unlikely that step defects[37–39], could explain these observations. The fact that this uniaxial anisotropy is dominant in thick LSMO films suggest that some kind of bulk structure established firstly at the step boundary, and then propagates as the LSMO grows[35].

Each of the curves in Fig.(4) has a different dc-offset, which does not depend on LSMO thickness in a systematic way. The most likely explanation for this is either differences in saturation magnetisation or pinning and out of plane anisotropy originating at the ferroelectric interface. Without the additional FEX modes for the in-plane data it is difficult to assess the contribution made by the ferroelectric layer to in-plane surface anisotropies.

FMR and FEX modes were seen in out-of-plane configuration measurements for some films. The lack of an FEX mode for in-plane measurements, and its presence in out-of-plane resonance measurements, indicate that surface pinning is most effective in the out-of-plane direction. When the surface pinning originates from an easy axis out-of-plane anisotropy, it has been shown that both dynamic components of magnetisation are pinned when the out-of-plane configuration, but that only one component is pinned when the magnetisation is in-plane[40]. As shown in Fig.(5) there is a strong FMR mode which is

present in all films and a FEX mode is observed in some films.

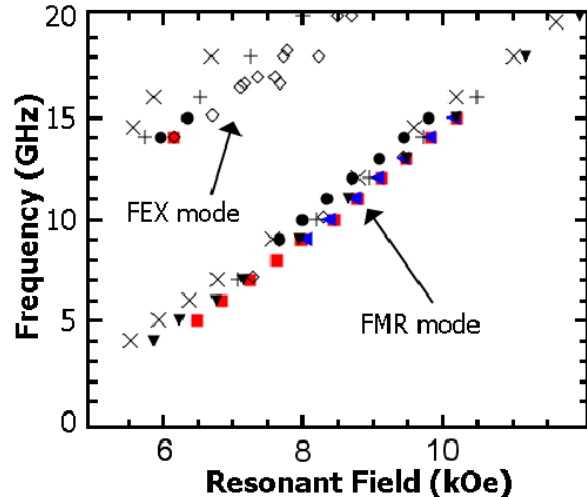


FIG. 5. Out-of-plane configuration resonant field H_f vs driving frequency ω is shown for a variety of different films. LSMO(30nm) (solid circles), LSMO(38.9) (solid squares and empty diamonds), LSMO(61.9nm) (solid sideways triangles), LSMO(55nm)/BFO(17nm) (solid down triangles), LSMO(54.8nm)/BFO(24nm) (plus symbols), LSMO(45nm)/PZT(20nm) (cross symbols). One collection of data originates from the FMR mode (as shown) and the other collection of points are from the FEX mode. By fitting a linear function to these data, gyromagnetic ratio γ and effective internal field H_{eff} may be extracted.

By fitting straight lines to the data in Fig.(5) we may extract γ and H_{eff} from Eq.(1). A comparison of these parameters for the different films is shown in Tab.(I).

The gyromagnetic ratio γ is extracted from the slope of the $\omega(H_R)$ data given in Fig.(5). H_{eff} is measured by the intercept with $\omega = 0$ for out-of-plane measurements. While the monolayer LSMO shows a net decrease in $H_{eff}(FMR)$ with thickness, indicating a reduction in out-of-plane anisotropies, the addition of a ferroelectric layer significantly changes H_{eff} . It should be noted that the PZT seems to much more strongly affect the magnetic parameters than BFO.

VI. SPIN WAVE STIFFNESS

We now discuss determination of D. We define the gap between effective fields for the two modes ΔH_{eff} as:

$$\begin{aligned} \Delta H_{eff} &= H_{eff}(FEX) - H_{eff}(FMR) \\ &= D (k_{oop}^2(FEX) - k_{oop}^2(FMR)) \end{aligned} \quad (4)$$

Eq.(4) does not contain contributions from $\mu_0 M_S - H_{oop}$, as this contributes equally to both $H_{eff}(FMR)$ and $H_{eff}(FEX)$.

Sample	$\gamma(FMR) \times 10^{10}$	$\gamma(FEX) \times 10^{10}$	$H_{eff}(FMR)$	$H_{eff}(FEX)$
STO/LSMO(30nm)	2.79	2.79	-4425	-956
STO/LSMO(38.9nm)	2.67	2.67	-4624	-973
STO/LSMO(61.9nm)	2.83	-	-4891	-
STO/LSMO(55nm)/BFO(18nm)	2.63	-	-4442	-
STO/LSMO(54.8nm)/BFO(24nm)	2.64	2.64	-4423	-437
STO/LSMO(45nm)/PZT(20nm)	2.63	2.63	-4089	176

TABLE I. Displayed are the extracted gyromagnetic ratio γ and effective internal field H_{eff} from data shown in Fig.(5). We attribute the distribution of γ to scatter in weak ferromagnetic resonance signals. Uncertainty in H_{eff} is ± 50 Oe, and originates from the remnant magnetic field in our electromagnet pole pieces and the imperfect lineshapes of the FMR signal. Also there exists large differences between the effective fields in the single layer LSMO and capped LSMO films. In particular, films with a more positive H_{eff} must possess stronger out-of-plane bulk anisotropies or pinning. Differences in H_{eff} for the FMR and FEX modes demonstrate that interface pinning must be playing a role in these films. For empty entries, no FEX mode was observed.

Tab.(II) lists the results of this gap for films in which the FEX mode was observed, and also for estimates of what these values should be assuming no interface pinning and the literature value of $D_{lit} = 1.7965 \times 10^{-17} \text{ T m}^2$ (or in the units for exchange stiffness $D_{lit} = 104 \text{ meV \AA}$). We note that the spin wave constant D used in the Kittel equation has units T m^2 and spin wave stiffness $D_{stiffness}$ possesses units J m^2 [11]. Converting between the two uses the following:

$$D = \frac{D_{stiffness}}{\mu_B}$$

We see immediately that there is a large discrepancy between the observed and predicted ΔH_{eff} . It is not possible from observations of two standing spin wave modes to identify separately pinning at each interface. We thus consider two extreme situations: complete pinning at the ferroelectric interface only (single sided pinning) and complete pinning at both interfaces (double sided pinning)[41]. D values deduced from measured ΔH_{eff} gaps in 38.9nm LSMO films for extreme pinning conditions are given in Tab.(III). The case where D_{lit} accounts for ΔH_{eff} can only occur for double sided pinning. In the case where extreme single sided magnetisation pinning exists, an exchange constant value of at least $1.49 \times D_{lit}$ is needed. Finally the case where ΔH_{eff} can be explained without any interface pinning is only possible for $2.98 \times D_{lit}$. Most likely, a combination of both a larger D combined with some pinning from both interfaces would account for the D value we find. In addition, there is clearly a much greater ΔH_{eff} gap for the films with a capping ferroelectric, especially for the PZT capped film. This indicates a significant out-of-plane interface pinning which originates from the ferroelectric layer.

VII. SUMMARY

Ferromagnetic resonance was used as a sensitive probe of both in-plane and out-of-plane anisotropies in multilayer LSMO/BFO and LSMO/PZT films. We have shown that some interface pinning must be playing a role in magnetisation dynamics. Interestingly, BFO seems to have little influence on the magnetisation of LSMO. We see no evidence of exchange bias[5, 6], though this may be because of the relatively thick LSMO layer dominating the magnetisation dynamics. The fast growth rate of BFO in comparison to[5] may also be an important factor in growing suitable BFO to couple to the ferromagnet. Electric fields were applied across the BFO layer and resonance experiments were carried out, but no shifts in FMR resonances were observed. From our data, it is quite difficult to extract separate pinning effects at each interface. However, a lower bound for D can be set given various assumptions about pinning at the interface. We find that complete pinning at both interfaces gives D for our films the same as literature D_{lit} .

Uniaxial and biaxial in-plane anisotropies appear to be unrelated to the capping ferroelectric layer are observed, and there may exist a thickness of LSMO about which a transition between anisotropies might take place. Our data indicates that the uniaxial contribution to anisotropy relative to the biaxial component increases as the ferromagnet thickness increases, for LSMO films grown on STO(100), unlike that found for LSMO grown on other substrates[8].

ACKNOWLEDGMENTS

We acknowledge the support of the ARC, University of Western Australia, DEST and the DIISR Australia India Strategic Research Fund ST020078.

[1] Z. Shi, C. Wang, X. Liu, and C. Nan, Chinese Sci. Bull. **53**, 2135 (2008).

[2] S. Majumdar, R. Laiho, P. Laukkanen, I. J. Väyrynen,

	ΔH_{eff} (experimental)	ΔH_{eff} (no pinning, D_{lit})
LSMO(30nm)	3651	1970
LSMO(38.9nm)	3496	1171
LSMO(45nm)/PZT(20nm)	4265	875
LSMO(54.8nm)/BFO(24nm)	3986	590

TABLE II. Experimentally found ΔH_{eff} are shown in the left column, in units of Oe and with an error of ± 50 . The right hand column displays calculated ΔH_{eff} for the thicknesses of LSMO using the literature value of $D_{lit} = 1.7965 \times 10^{-17} \text{T m}^2$ and no interface pinning. Note that experimental ΔH_{eff} pinning from different capping layers appears significant.

	no pinning	max single sided pinning	max double sided pinning
D_{lit}	1171	2343	3515
1.49 D_{lit}	1745	3491	5237
2.98 D_{lit}	3491	6983	10475

TABLE III. Theoretically calculated ΔH_{eff} (in Oe) for a 38.9nm LSMO film given various extreme interface pinning conditions (top row), and different values of D (with respect to $D_{lit} = 1.7965 \times 10^{-17} \text{T m}^2$). It is important to note the actual $\Delta H_{eff} = 3496$ Oe. Assuming that the entirety of pinning originates from one interface, $D = 1.49 D_{lit}$ as indicated in the table.

- H. S. Majumdar, and R. Österbacka, Appl. Phys. Lett. **89**, 122114 (2006).
- [3] F. J. Wang, C. G. Yang, Z. V. Vardeny, and X. G. Li, Phys. Rev. B **75**, 245324 (Jun 2007).
- [4] J.-H. Park, E. Vescovo, H. J. Kim, C. Kwon, R. Ramesh, and T. Venkatesan, Nature (London) **392**, 794 (1998).
- [5] L. W. Martin, Y.-H. Chu, M. B. Holcomb, M. Huijben, P. Yu, S.-J. Han, D. Lee, S. X. Wang, and R. Ramesh, Nano Lett. **8**, 2050 (2008).
- [6] J. Dho, X. Qi, H. Kim, J. MacManus-Driscoll, and M. Blamire, Adv. Mater. **18**, 1445 (2006).
- [7] S. M. Wu, S. A. Cybart, P. Yu, M. D. Rossell, J. X. Zhang, R. Ramesh, and R. C. Dynes, Nat. Mater. **9**, 756 (2010).
- [8] H. Nishikawa, E. Houwman, H. Boschker, M. Mathews, D. H. A. Blank, and G. Rijnders, Appl. Phys. Lett. **94**, 042502 (jan 2009).
- [9] I. Gomes, B. Almeida, A. Lopes, J. Araújo, J. Barbosa, and J. Mendes, J. Magn. Magn. Mater **322**, 1174 (2010), ISSN 0304-8853.
- [10] M. Huijben, L. W. Martin, Y.-H. Chu, M. B. Holcomb, P. Yu, G. Rijnders, D. H. A. Blank, and R. Ramesh, Phys. Rev. B **78**, 094413 (Sep 2008).
- [11] M. Golosovsky, P. Monod, P. K. Muduli, and R. C. Budhani, Phys. Rev. B **76**, 184413 (Nov 2007).
- [12] A. A. Sidorenko, G. Allodi, R. De Renzi, G. Balestrino, and M. Angeloni, Phys. Rev. B **73**, 054406 (Feb 2006).
- [13] Y. Suzuki, H. Y. Hwang, S.-W. Cheong, and R. B. van Dover, Appl. Phys. Lett. **71**, 140 (1997).
- [14] S. E. Lofland, S. M. Bhagat, Q. Q. Shu, M. C. Robson, and R. Ramesh, Appl. Phys. Lett. **75**, 1947 (1999).
- [15] J. Dho and N. Hur, J. Magn. Magn. Mater. **318**, 23 (2007), ISSN 0304-8853.
- [16] L. B. Steren, M. Sirena, and J. Guimpel, J. Appl. Phys. **87**, 6755 (may. 2000).
- [17] M. Ziese, I. Vrejoiu, E. Pippel, P. Esquinazi, D. Hesse, C. Etz, J. Henk, A. Ernst, I. V. Maznichenko, W. Hergert, and I. Mertig, Phys. Rev. Lett. **104**, 167203 (Apr 2010).
- [18] C. Thiele, K. Dörr, S. Fähler, L. Schultz, D. C. Meyer, A. A. Levin, and P. Paufler, Applied Physics Letters **87**, 262502 (2005).
- [19] M. C. Martin, G. Shirane, Y. Endoh, K. Hirota, Y. Moritomo, and Y. Tokura, Phys. Rev. B **53**, 14285 (Jun 1996).
- [20] L. Vasiliu-Doloc, J. W. Lynn, Y. M. Mukovskii, A. A. Arsenov, and D. A. Shulyatev, J. Appl. Phys. **83**, 7342 (1998).
- [21] A. H. Moudden, L. Vasiliu-Doloc, L. Pinsard, and A. Revcolevschi, Physica B **241-243**, 276 (1997).
- [22] W. Stoocklein, S. S. P. Parkin, and J. C. Scott, Phys. Rev. B **38**, 6847 (1988).
- [23] R. D. McMichael, M. D. Stiles, P. J. Chen, and W. F. Egelhoff, Phys. Rev. B **58**, 8605 (1998).
- [24] C. Kittel, Introduction to Solid State Physics, 8th ed. (John Wiley & Sons, Inc, 2005).
- [25] C. Kittel, Phys. Rev. **110** (1958).
- [26] J. M. H. Seavey and P. Tannenwald, Phys. Rev. Lett. **1**, 168 (1958).
- [27] M. Hambe, A. Petraru, N. A. Pertsev, P. Munrow, V. Nagarajan, and H. Kohlstedt, Adv. Func. Mater. **20**, 2436 (2010).
- [28] K. J. Kennewell, M. Kostylev, N. Ross, R. Magaraggia, R. L. Stamps, M. Ali, A. A. Stashkevich, D. Greig, and B. J. Hickey, J. Appl. Phys. **108** (2010).
- [29] M. Kostylev, Journal of Applied Physics **106**, 043903 (2009).
- [30] K. J. Kennewell, M. Kostylev, M. Ali, A. A. Stashkevich, R. Magaraggia, D. Greig, B. J. Hickey, and R. L. Stamps, arXiv: 1001.1837v1(2010).
- [31] W. S. Ament and G. T. Rado, Phys. Rev. **97**, 1558 (1955).
- [32] Y. V. Khivintsev, L. Reisman, J. Lovejoy, R. Adam, C. M. Schneider, R. E. Camley, and Z. J. Celinski, J. Appl. Phys. **108**, 023907 (2010).
- [33] P. Pincus, Phys. Rev. **118**, 658 (1960).
- [34] M. Mathews, F. M. Postma, J. C. Lodder, R. Jansen, G. Rijnders, and D. H. A. Blank, Appl. Phys. Lett. **87**, 242507 (dec. 2005).
- [35] Z. H. Wang, G. Cristiani, and H. U. Habermeier, Appl. Phys. Lett **82**, 3731 (2003).
- [36] P. Perna, E. Jiménez, F. J. Teran, L. Méchin, N. Mikuszeit, J. Camarero, and R. Miranda, arXiv:1005.0553v1(2001).
- [37] R. Arias and D. L. Mills, Phys. Rev. B. **59**, 11871 (1999).
- [38] D. S. Chuang, C. A. Ballentine, and R. C. O'Handley, Phys. Rev. B **49**, 15084 (Jun 1994).

- [39] L. Néel, J. Phys. Radium **15**, 225 (1954).
- [40] N. Salansky and M. Erukhimov, Physical properties and application of magnetic films (Moscow: Nauka, 1975).
- [41] We note that if complete pinning does occur at both interfaces, then the first exchange mode becomes symmet-

ric and will not be excited by a uniform driving field. In our experiment, only the conductivity would cause a non-uniform driving field, and this effect is estimated to be quite weak for LSMO. Hence a first exchange mode which experiences double sided pinning would be extremely difficult to detect. In our estimation of the theoretical range of D we neglect this fact.